Article

Direct Imaging of Surface Topology and Pore System of Ordered Mesoporous Silica (MCM-41, SBA-15, and KIT-6) and Nanocast Metal Oxides by High Resolution Scanning Electron Microscopy

Harun Tu#ysu#z, Christian W. Lehmann, Hans Bongard, Bernd Tesche, Roland Schmidt, and Ferdi Schu#th

J. Am. Chem. Soc., **2008**, 130 (34), 11510-11517 • DOI: 10.1021/ja803362s • Publication Date (Web): 31 July 2008

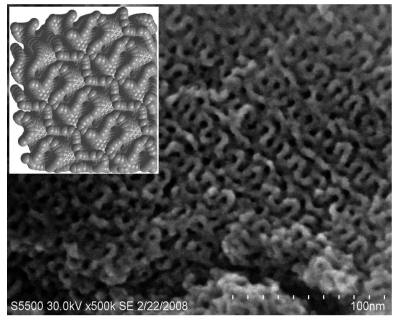

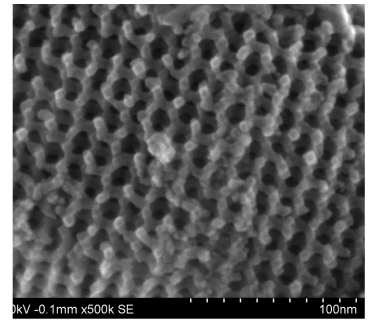

More About This Article

Additional resources and features associated with this article are available within the HTML version:

- Supporting Information
- Links to the 2 articles that cite this article, as of the time of this article download
- Access to high resolution figures
- Links to articles and content related to this article
- Copyright permission to reproduce figures and/or text from this article

View the Full Text HTML

J|A|C|S
ARTICLES

Published on Web 07/31/2008

Direct Imaging of Surface Topology and Pore System of Ordered Mesoporous Silica (MCM-41, SBA-15, and KIT-6) and Nanocast Metal Oxides by High Resolution Scanning Electron Microscopy

Harun Tüysüz,[†] Christian W. Lehmann,[†] Hans Bongard,[†] Bernd Tesche,[†] Roland Schmidt,[‡] and Ferdi Schüth*[,†]

MPI für Kohlenforschung Kaiser-Wilhelm-Platz 1, D-45470 Mülheim an der Ruhr, Germany, and Hitachi High-Technologies Europe GmbH, Europark Fichtenhain A 12, 47807, Krefeld, Germany

Received May 6, 2008; E-mail: schueth@mpi-muelheim.mpg.de

Abstract: We report here a detailed study on the surface topology of well-known ordered mesoporous silica (SBA-15, MCM-41, and KIT-6) and a series of nanocast Co_3O_4, $Co_3O_4/CoFe_2O_4$ composites by high resolution scanning electron microscopy (HR-SEM). Images of the MCM-41 structure were obtained at a resolution of the pore size, as well as a real space image of the gyroid silica surface of KIT-6 for two different aging temperatures, clearly revealing the differences of the aging procedures. By using the low voltage HR-SEM technique with extremely high resolution, we could very clearly show the influence of the template properties on the structure of the nanocast metal oxides.

Introduction

Mesoporous silica and other mesoporous oxides are useful in a variety of applications, including catalysis, sorption, photonics, and electronics.[1−3] The interest in such ordered mesoporous systems results from their interesting framework topologies, high surface area, and controllable pore size and pore volume. Ordered mesoporous materials can be fabricated via soft templating (cooperative assembly) and hard templating (nanocasting) pathways.[4−7] The two most often investigated pore topologies are the hexagonally packed cylindrical pores, as found in MCM-41 and SBA-15, and the complex pore system present in the $Ia\bar{3}d$ structure. This structure is bicontinuous, containing two enantiomeric pore systems, separated by a minimal surface composed of silica. This minimal surface corresponds to the G-surface, which was, for instance, described by S. Andersson as an important structural feature of crystals and liquid crystals.[8,9]

For most applications, the nature of the pore system and also the access of the pore system from the surface are highly important. This, however, is not easy to analyze. Transmission electron microscopy gives limited information about the shape, connectivity, and three-dimensional (3D) orientation of the pores, because it essentially provides a 2D projection of the 3D material. Nevertheless, it can be used to obtain 3D-information in special cases, as for instance shown by Liu et al. who studied the 3D-shape of SBA-15 and nanocast Pt nanowires by high-resolution electron microscopy (HREM).[10] Much more detailed 3D information, however, can be obtained in the tomography mode. For this, a series of TEM images of the same position is taken at different tilt angles. Computational image reconstruction allows one to obtain a 3D representation.[11,12] A 3D-TEM study of the shape of mesopores in SBA-15 was published by Janssen et al.,[13] as well as an analysis of the distribution of gold nanoparticles dispersed on SBA-15.[14] They showed that SBA-15 has a high degree of ordering of the mesopores on a microscopic scale, and irregularly curved pores on a macroscopic scale. This method is very powerful in elucidating 3D information, but application of the technique is rather complex, and beam damage is a potential problem, because the same sample position is exposed to the beam for an appreciable period of time.

Scanning electron microscopy (SEM) has advantages as compared to TEM and 3D-TEM, especially for studying the morphology of samples. SEM is a comparatively simple method and does not require substantial sample preparation and long

[†] MPI für Kohlenforschung.
[‡] Hitachi High-Technologies Europe GmbH.

(1) Taguchi, A.; Schüth, F. *Microporous Mesoporous Mater.* **2005**, *77*, 1.
(2) Davis, M. E. *Nature* **2002**, *417*, 813.
(3) He, X.; Antonelli, D. *Angew. Chem., Int. Ed.* **2002**, *41*, 214.
(4) Wan, Y.; Zhao, D. *Chem. Rev.* **2007**, *107*, 7.
(5) Lu, A. H.; Schüth, F. *Adv. Mater.* **2006**, *18*, 1793.
(6) Tiemann, M. *Chem. Mater.* **2008**, *20*, 961.
(7) Tüysüz, H.; Salabas, E. L.; Weidenthaler, C.; Schüth, F. *J. Am. Chem. Soc.* **2008**, *130*, 280.
(8) Hyde, S.; Andersson, S.; Larsson, K. *The Language of Shape: The Role of Curvature in Condensed Matter: Physics, Chemistry and Biology*; Elsevier: Amsterdam, 1996; 396 pp.
(9) Anderson, M. W. *Zeolites* **1997**, *19*, 220.
(10) Liu, Z.; Terasaki, O.; Ohsuna, T.; Hiraga, K.; Shin, J. H.; Ryoo, R. *ChemPhysChem* **2001**, *2*, 229.
(11) Ersen, O.; Hirlimann, C.; Drillon, M.; Werckmann, J.; Tihay, F.; Pham-Huu, C.; Crucifix, C.; Schulz, P. *Solid State Sci.* **2007**, *9*, 1088.
(12) Koster, A. J.; Ziese, U.; Verkleij, A. J.; Hansen, A. H.; de Jong, K. P. *J. Phys. Chem. B* **2000**, *104*, 9368.
(13) Janssen, A. H.; Van der Voort, P.; Koster, J. A.; de Jong, K. P. *Chem. Commun.* **2002**, 1632.
(14) Janssen, A. H.; Yang, C. M.; Wang, Y.; Schüth, F.; Koster, A. J.; de Jong, K. P. *J. Phys. Chem. B* **2003**, *107*, 10552.

10.1021/ja803362s CCC: $40.75

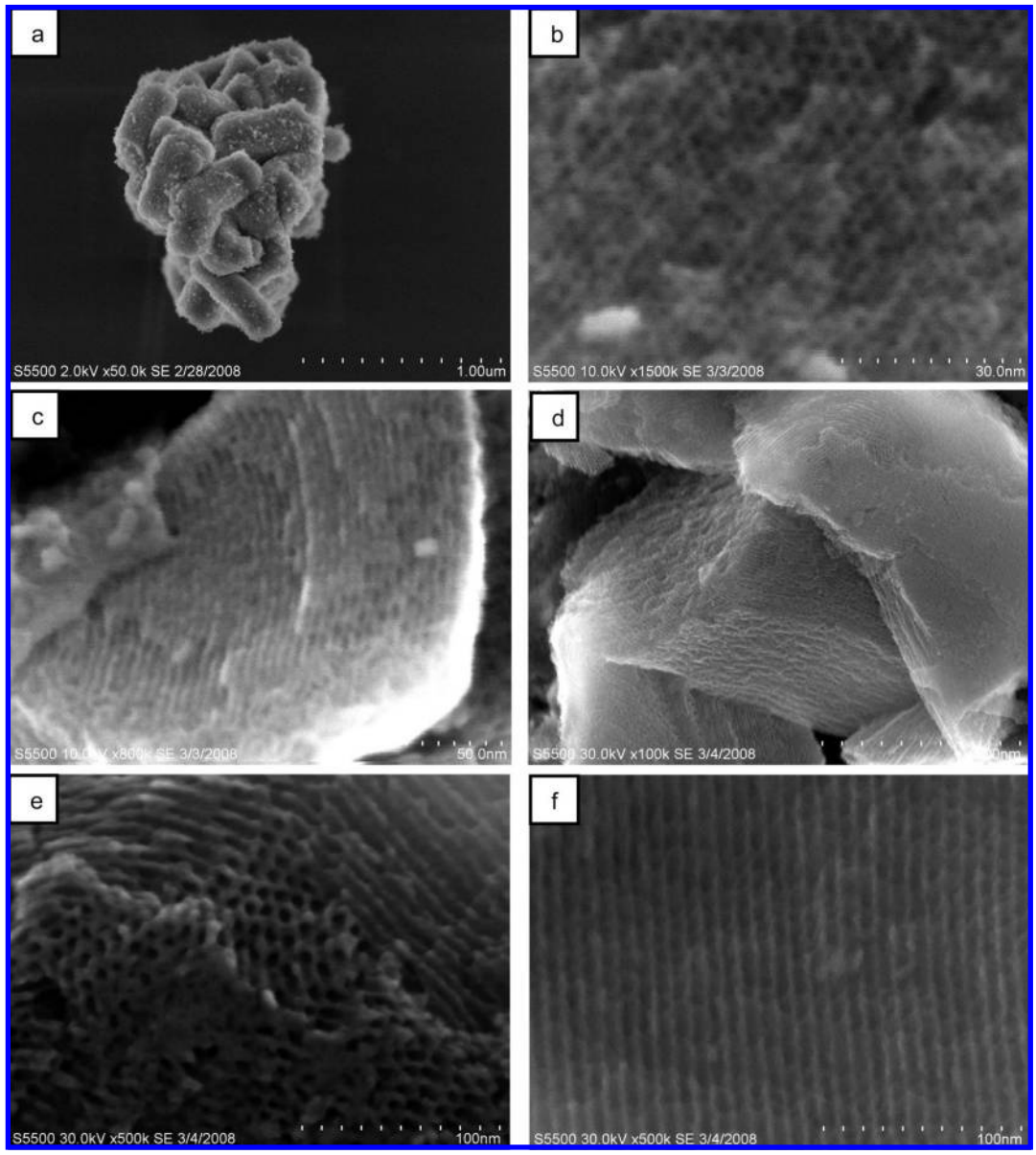

Figure 1. HRSEM images of hexagonally ordered MCM-41 (a,b,c) and SBA-15 (d,e,f).

analysis times. One of the limitations of this technique until recently was its low resolution. However, nowadays it is possible to investigate the surface of porous materials with high resolution-SEM (HR-SEM), working at very low currents and voltages.[15] Che et al. reported details of the surface structures of SBA-15 and its carbon replica CMK-5, by using HR-SEM and scanning transmission electron microscopy (STEM).[16] The presence of interconnections between the hexagonally packed mesoporous channels could be observed clearly. Using the same analysis method, but predominantly TEM, time-dependent structural changes in M41S mesoporous silica were analyzed, albeit at a resolution where the pore openings of the MCM-41 channels on the external surface could not be resolved.[17] Bore et al. investigated the role of the pore size and the structure on the thermal stability of the gold nanoparticles within mesoporous silica using HR-SEM. They showed the fine distribution of the gold nanoparticles in the channels of the SBA-15; however, the pore size of MCM-41 could not be resolved.[18]

In the following, we report a detailed structural investigation of ordered mesoporous silica and nanocast cubic ordered mesoporous Co_3O_4 and $Co_3O_4/CoFe_2O_4$ composites by HR-SEM. We have obtained unprecedented resolution of the surface and near surface regions of ordered mesoporous silica by HR-SEM. Co_3O_4 that was nanocast from KIT-6 aged at lower temperature mainly shows an uncoupled subframework, while Co_3O_4 that was prepared from KIT-6 with higher aging temperature shows a rather dense structure, formed by the two coupled subframeworks of the KIT-6 mold.

(15) Anderson, M. W.; Ohsuna, T.; Sakamoto, Y.; Liu, Z.; Carlsson, A.; Terasaki, O. *Chem. Commun.* **2004**, 907.
(16) Che, S.; Lund, K.; Tatsumi, T.; Iijima, S.; Joo, S. H.; Ryoo, R.; Terasaki, O. *Angew. Chem., Int. Ed.* **2003**, *42*, 2182.
(17) Diaz, I.; Perez-Pariente, J.; Terasaki, O. *J. Mater. Chem.* **2004**, *14*, 48.
(18) Bore, M. T.; Pham, H. N.; Switzer, E. E.; Ward, T. L.; Fukuoka, A.; Datye, A. K. *J. Phys. Chem. B* **2005**, *109*, 2873.

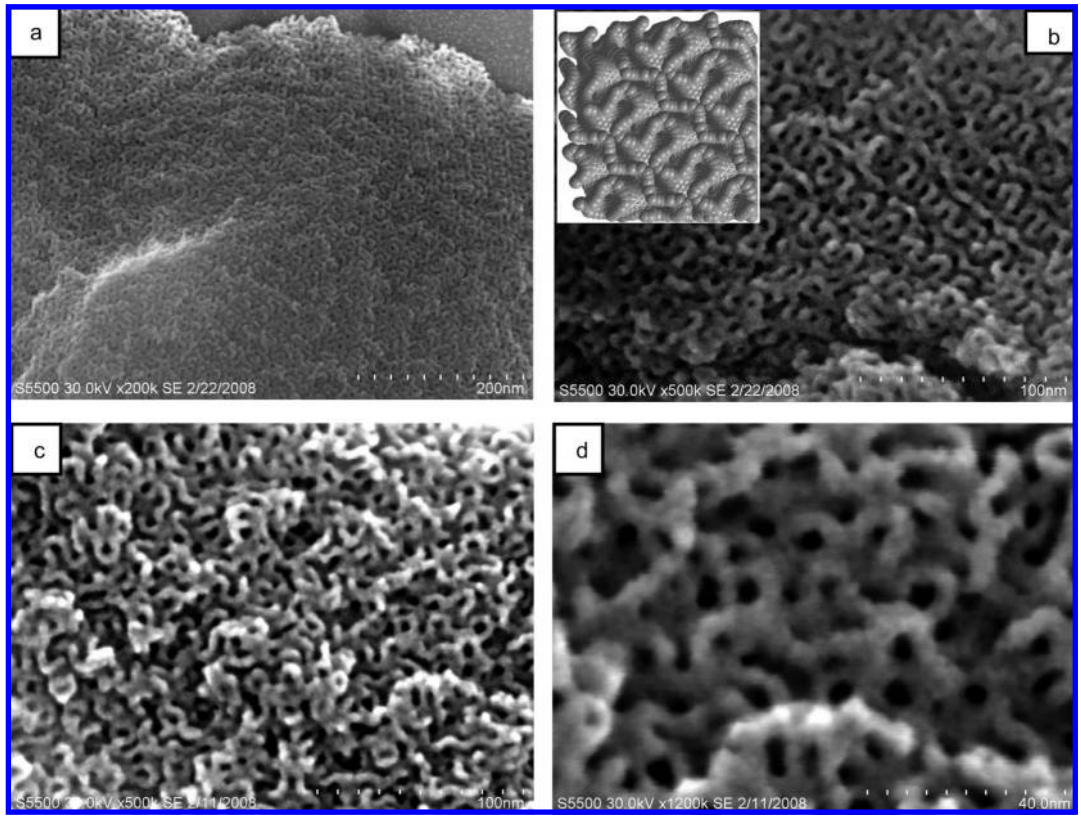

Figure 2. HR-SEM images of cubic ordered KIT-6 with 40 °C (a,b) and 100 °C (c,d) aging temperature. The inset in (b) shows a cross section through a model of the triply periodic surface Schoen G (gyroid) composed of 3 × 3 × 3 unit cells.

Table 1. Texture Parameters of KIT-6 and Nanocast Metal Oxides

	S_{BET} m^2 g^{-1}	V_T cm^3 g^{-1}	pore size nm
KIT-6-40	547	0.505	3.9
KIT-6-100	694	0.950	7.9
KIT-6-135	558	1.305	11.4
Co_3O_4-40	160	0.527	6.7
Co_3O_4-100	110	0.193	3.4
Co_3O_4-135	70	0.110	3.0
Co_3O_4−$CoFe_2O_4$	140	0.323	6.0

Experimental Section

Ordered mesoporous MCM-41,[19] SBA-15,[20] and KIT-6[21] were prepared according to literature procedures. The texture parameters of KIT-6 were varied by changing the hydrothermal synthesis temperature (aging temperature: 40, 100, and 135 °C). This material was used as a hard template to create ordered mesoporous Co_3O_4. In a typical synthesis, 0.5 g of KIT-6 was dispersed in 5 mL of 0.8 M $Co(NO_3)_2 \cdot 6H_2O$ in ethanol and stirred for 1 h at room temperature, and subsequently the ethanol was evaporated at 50 °C. The composite was calcined at 200 °C for 6 h. The composite was reimpregnated again, followed by calcination at 450 °C for 6 h. The silica template was then removed using 2 M NaOH aqueous solution, followed by several washing steps with water and a final drying step at 50 °C. The samples are denoted as Co_3O_4-*T*, where *T* indicates the aging temperature of the parent template. In the synthesis of mesoporous Co_3O_4−$CoFe_2O_4$, KIT-6 synthesized at 40 °C aging temperature was used as hard template. First, an ethanol solution of $Co(NO_3)_2 \cdot 6H_2O$ was impregnated into KIT-6, the solution was evaporated, and the sample was calcined at 200 °C for 6 h. After that, a mixture of $Co(NO_3)_2 \cdot 6H_2O$ and $Fe(NO_3)_3 \cdot 9H_2O$ (molar ratio Co/Fe = 2) in ethanol was impregnated into the sample, and this was subsequently calcined at 450 °C for 6 h. The rest of the procedure is identical to the synthesis of mesoporous Co_3O_4.

The XRD patterns were recorded on a Stoe θ/θ diffractometer in Bragg−Brentano geometry (Cu Kα radiation) at room temperature. Nitrogen adsorption isotherms were measured with an ASAP 2010 adsorption analyzer (Micromeritics) at liquid nitrogen temperature. Prior to the measurements, the samples were degassed at a temperature of 150 °C for 10 h. Total pore volumes were determined using the adsorbed volume at a relative pressure of 0.97. BET (Brunauer−Emmett−Teller) surface area was determined from the relative pressure range 0.06−0.2. Pore size distribution (PSD) curves were calculated by the BJH (Barrett−Joyner−Halenda) method from the adsorption branch. High resolution transmission electron microscopy (HR-TEM) images of samples were obtained with an HF-2000 microscope (Hitachi) equipped with a cold field emission gun. The acceleration voltage was 200 kV. Samples were prepared on carbon film covered grids. High resolution scanning electron microscopy (HR-SEM) and scanning transmission electron microscopy (STEM) images of the samples were taken using a Hitachi S-5500 ultrahigh resolution cold field emission scanning electron microscope operated at 2, 10, and 30 kV. The S-5500 is unique in that it combines a cold FEG with an in-lens electron optic, a side empty sample holder (similar to those used for TEM), and a patented energy filter for secondary electron (SE) selection, together with an in-lens SE detector geometry. It permits also three-dimensional morphological observation down to atomic or molecular level of structures of various materials, far surpassing the performance of any conventional SEM. A new Duo-STEM bright field/dark field detector allows simultaneous imaging, while offering an adjustable detection angle for the dark field image. All samples were prepared on a lacey carbon film supported by a copper grid.

(19) Cai, Q.; Lin, W. Y.; Xiao, F. S.; Pang, W. Q.; Chen, X. H.; Zou, B. S. *Microporous Mesoporous Mater.* **1999**, *33*, 187.
(20) Choi, M.; Heo, W.; Kleitz, F.; Ryoo, R. *Chem. Commun.* **2003**, 1340.
(21) Kleitz, F.; Choi, S. H.; Ryoo, R. *Chem. Commun.* **2003**, 2136.

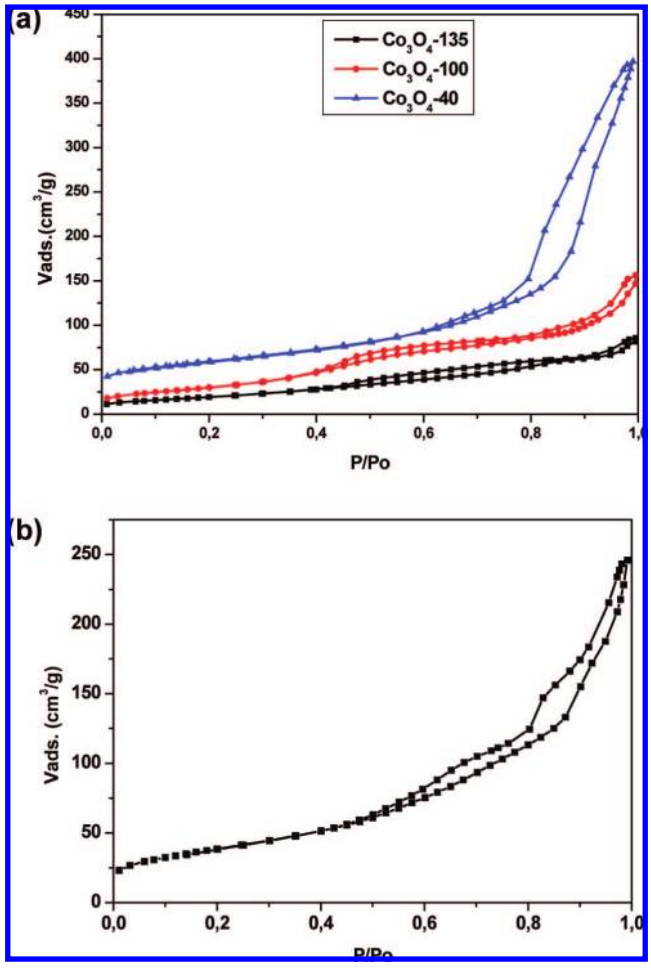

Figure 3. Nitrogen adsorption−desorption isotherms of the Co_3O_4 series (a) and Co_3O_4−$CoFe_2O_4$ composite (b).

The obtained images were analyzed using the Scandium 5.0 software package from Soft Imaging System GmbH.

Results and Discussion

Ordered mesoporous silicas were characterized with XRD, N_2-sorption, and HR-SEM. Low angle XRD patterns of all samples indicate well-ordered structures (Supporting Information Figure S1). Texture parameters of the silicas were determined by N_2-sorption (Supporting Information Figure S2). MCM-41 has a Brunauer−Emmett−Teller (BET) surface area of 1538 m^2/g, a pore volume of 0.922 cm^3/g, and a pore size of 2 nm obtained from the adsorption branch using the BJH algorithm. For SBA-15 and KIT-6, the aging temperature can be used to control pore size and pore volume to a certain extent. With increasing aging temperature, pore size and pore volume of SBA-15 and KIT-6 samples increased while silica wall thickness decreased. SBA-15 that was aged at 90 °C has a BET surface area of 772 m^2/g, pore volume of 0.849 cm^3/g, and pore size of 6.6 nm, while KIT-6 (aging temperature 100 °C) has a BET surface area of 694 m^2/g, pore volume of 0.950 cm^3/g, and pore size of 7.9 nm. KIT-6 with lower aging temperature (40 °C) has a BET surface area of 559 m^2/g, a pore volume of 0.505 cm^3/g, and a pore size of 3.9 nm.

The topology of the ordered mesoporous silica was investigated by HR-SEM. The design of the S-5500 permits the observation of insulator without depositing any metals on the sample, even at 30 kV acceleration voltage. However, large particles still tend to become charged; therefore, in the case of MCM-41 (investigated as synthesized without any grinding or crashing), the voltage was lowered. Figure 1 shows HR-SEM images of hexagonally ordered mesoporous MCM-41 (a,b,c) and SBA-15 (d,e,f). Image analysis gave an MCM-41 particle size in the range of 400 (±100) nm, a pore size of 2 nm, and wall thickness of around 1.8 nm. Figure 1b,c indicates the regular hexagonal array of uniform channels in the MCM-41. On top of the hexagonally ordered channels of the MCM-41, some amorphous silica particles can be seen. It is also obvious that the channels are not perfect, but seem to contain defects and constrictions. In addition, one can clearly see that the channel openings are fully exposed at the surface of the individual particles. The channels seen sideways (Figure 1c) also seem to be accessible along their long axis. It is not clear whether such defects extend deeper into the crystal, because SEM does not provide bulk information, but if they did, this would allow unrestricted access to the pore system. Such or similar defects may be the origin for the unexpected diffusion of dye molecules perpendicular to the axis of helical mesoporous silica fibers, which has recently been described.[22] The surface perpendicular to the channel direction (Figure 1b) is not smooth, but irregularly shaped. Because there is no periodicity in the *c*-direction, no obvious plane for clean termination in this direction exists, and this result is therefore not surprising. However, the shape of MCM-41 particles depends on synthetic conditions, and thus this may be different for other preparations. The cut parallel to the channel direction has a distinctly different appearance (Figure 1c). Terraces can be seen, formed by a number of channels in the same plane. However, some of these channels are open along their axis, so termination is not fully perfect.

As compared to MCM-41, SBA-15 has bigger pore size and thicker silica walls, clearly visible in the HR-SEM images (Figure 1e,f). Pore size and silica wall thickness of SBA-15 were estimated at around 6 and 4 nm, respectively. Figure 1d confirms that the SBA-15 particles consist of many different domains, which are hexagonally ordered on a short length scale but highly curved on the particle level, in agreement with the tomography study.[13] The surface in parts consists of the channel openings in hexagonal arrangement, of channels where the inside is exposed along the channel axis, and of sections that seem to be covered by a relatively smooth silica layer.

The pore system of KIT-6 had so far not been analyzed by HR-SEM. We have studied KIT-6 samples, which had been aged at different aging temperature. KIT-6 has $Ia\bar{3}d$ symmetry and two channel systems that are connected with each other through smaller pores, at least if the synthesis temperature is sufficiently high.[23] With increasing aging temperature of KIT-6, the interconnectivity between these two channel systems increases. This can directly be observed in the HR-SEM images. Figure 2 shows images of KIT-6 aged at 40 °C (a,b; a model for cubic structure with $Ia\bar{3}d$ symmetry is given in the inset of Figure 2b) and 100 °C aging temperature (c,d). The surface of these materials appears relatively disordered, which is due to the fact that in most cases the surface is not terminated along crystallographically well-defined planes, but is rather corrugated. However, in some sections, more regular surface structures could clearly be observed, for instance, in Figure 2b. The appearance

(22) Stempniewicz, M.; Khalil, A. S. G.; Rohwerder, M.; Marlow, F. *J. Am. Chem. Soc.* **2007**, *129*, 10561.
(23) Kim, T. W.; Kleitz, F.; Paul, B.; Ryoo, R. *J. Am. Chem. Soc.* **2005**, *127*, 7601.

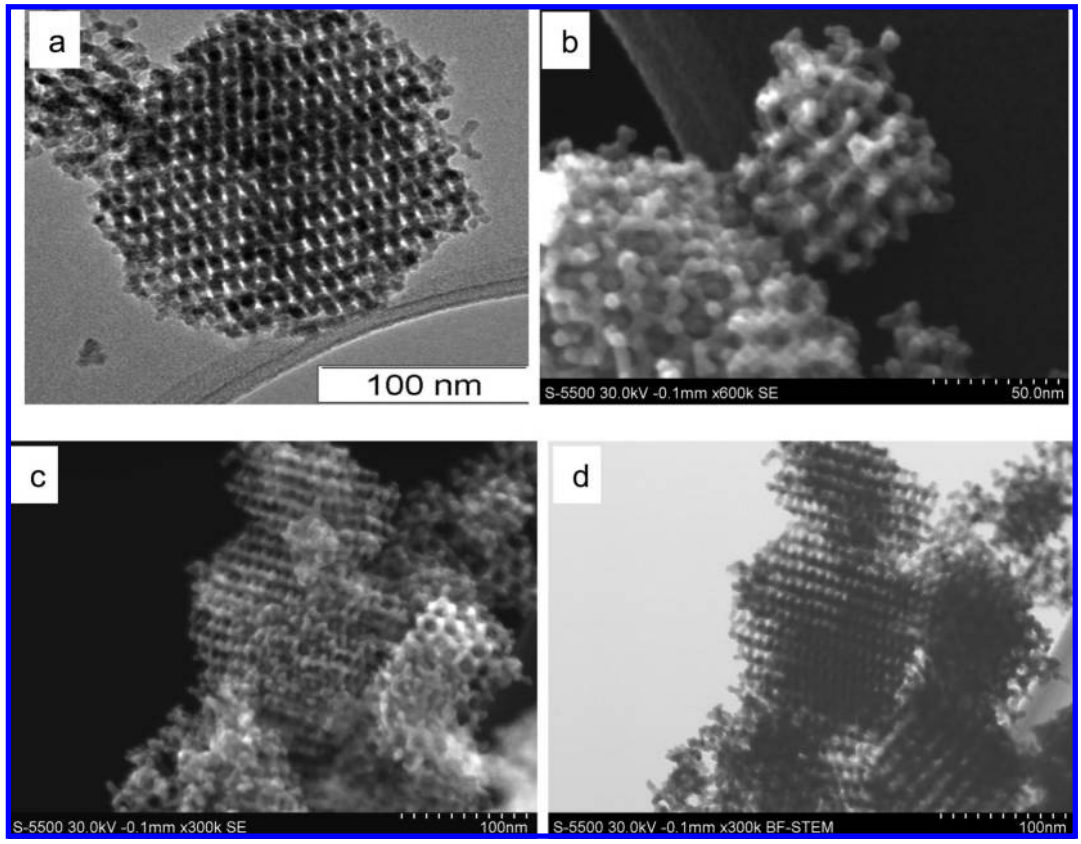

Figure 4. HR-TEM (a), HR-SEM (b,c), and STEM (d) images of Co_3O_4-40.

of this image could be simulated by a cut through the perfect $Ia\bar{3}d$ structure. The inset in Figure 2b shows a cross section through a model of the triply periodic surface Schoen G (gyroid) composed of $3 \times 3 \times 3$ unit cells.[24] The cross section is parallel to the 211 lattice plane at a distance of 1.674 Å from the origin placed at (0,0,0), and the similarity between the SEM image and this simulated image is obvious. Also, in other parts of the images, 3-fold local symmetry, as expected from the cubic structure, is visible, but long-range order is rarely found, due to the uneven surface termination and the domain structure of the material. Nevertheless, full and unrestricted access of the pore system from the surface is clearly demonstrated by the SEM images.

Pore size and silica wall thickness can be determined easily from the images. KIT-6 with lower aging temperature has a pore size of around 3.8 nm and a silica wall thickness of 5 nm, while KIT-6 with 100 °C aging temperature has pore size and silica wall thickness of around 7.5 and 3.5 nm, respectively. The wall of KIT-6 aged at 40 °C aging temperature appears much denser and more solid, while the high temperature aged KIT-6 sample has a rather open pore structure, in which many small openings connecting the two main pore systems can be seen.

KIT-6 aged at different temperatures was used as hard template to prepare ordered mesoporous metal oxide. The texture parameters of the templates and nanocast metal oxides that were determined by nitrogen physisorption measurements are summarized in Table 1. Depending on the type of the template, the porosity, surface area, and particle size of the mesoporous Co_3O_4 can be controlled up to a certain extent. The template with smaller pore size (thicker silica wall) gives a replica with bigger pore size. As one can see from Table 1, with decreasing aging temperature of the template, surface area, pore volume, and pore size of the nanocast Co_3O_4 increase. The Co_3O_4-40 and Co_3O_4/$CoFe_2O_4$ composites were fabricated from KIT-6-40; they both have similar texture parameters. The isotherms of the mesoporous metal oxides are given in Figure 3. They are all type IV isotherms, which is characteristic for mesoporous materials. However, as expected from the strongly differing properties of the parent KIT-6 samples, the sorption isotherm of the Co_3O_4-40 has a very pronounced capillary condensation step, while this is almost invisible for the Co_3O_4-135, corresponding to the small wall thickness of the parent material.

As observed before in studies on CMK-1[25] and Co_3O_4[26] replication from silica templates, lower aging temperatures during the preparation of the template (MCM-48 or KIT-6) may result in a decreased formation of interconnectivities within the gyroid structure. In this case, low angle XRD pattern of nanocast cubic ordered mesoporous Co_3O_4 shows an additional [110] peak (for XRD patterns, see Supporting Information Figure S3), indicating reduced symmetry of the nanocast material due to the fact that the parts of the enantiomeric pore systems of the parent silica are filled independently of each other. However, with increasing aging temperature this peak loses the intensity and after a certain aging temperature disappears. This may be

(24) The coordinates of 1088 selected points on this surface were taken from http://www.iwr.uniheidelberg.de/organization/bioms/schwarz/BicontinuousPhases/G/g.of and have been represented as spheres using the program Diamond Ver.3.1d, Klaus Brandenburg, Crystal Impact GbR, Bonn, Germany, 1997−2006.

(25) Solovyov, L. A.; Zaikovskii, V. I.; Shmakov, A. N.; Belousov, O. V.; Ryoo, R. *J. Phys. Chem. B* **2002**, 12198.

(26) Rumplecker, A.; Kleitz, F.; Salabas, E. L.; Schüth, F. *Chem. Mater.* **2007**, *19*, 485.

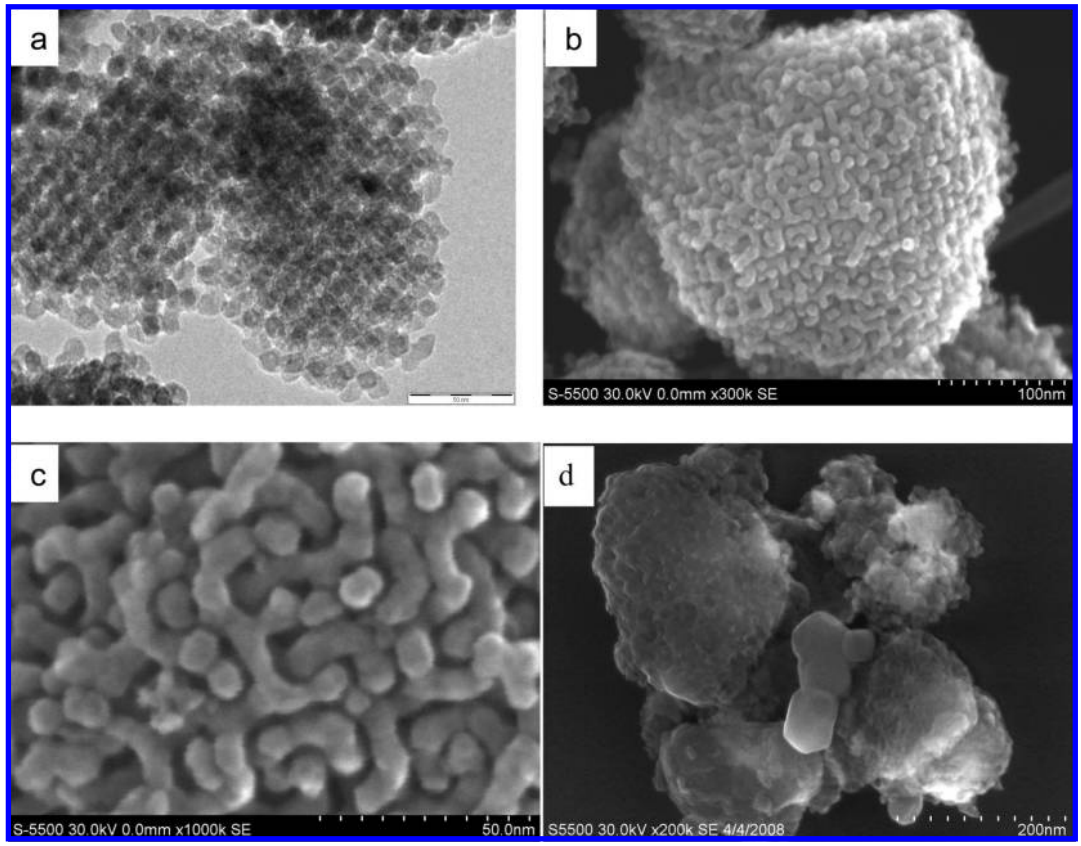

Figure 5. HR-TEM (a), HR-SEM (b,c) images of Co_3O_4-100, and Co_3O_4-KIT-6 composite (d).

attributed to a concerted filling of the two pore systems in parts of the parent material, which maintains the original symmetry. Because the pore system of the parent is never completely filled in a nanocasting process, the nanocast material has to aggregate during the curing in parts of the parent pore system. If there are no interconnectivities between the enantiomeric pore systems, this aggregation process takes place in both pore systems independently, and the structure with the reduced symmetry is formed. However, if there are enough interconnecting pores, material accretes in a concerted manner, and nucleation of the nanocast phase takes place with the product spanning both pore systems.

To study the topology and the porosity in more detail, HR-TEM and especially HR-SEM were used on these nanocast metal oxides. HR-TEM, HR-SEM, and STEM images of Co_3O_4-40 are shown in Figure 4a−d, respectively. While TEM reveals 2D projections of the material, SEM gives a three-dimensional impression of the pore structure, at least close to the surface of the material. The size of the individual crystallites making up the Co_3O_4-40 was estimated from TEM and SEM images, from the former only in two dimensions, and an average crystallite size of around 6 nm was estimated from both techniques. As has been discussed above, KIT-6 obtained at a low aging temperature of 40 °C has lower interconnectivity between the channels, and the two pore systems of the KIT-6 are hardly interconnected with each other. Therefore, Co_3O_4-40, which was fabricated from KIT-6 aged at low temperature, has partially uncoupled subframeworks. This phenomenon can be seen clearly from SEM images of Co_3O_4-40 (Figure 4b,c). This is due to the fact that the accretion of the cobalt material in the two different pore systems occurs largely independently, and thus extended structures are formed uncorrelated in most parts of the sample. This results in the formation of a very open pore system with the overall reduced symmetry, as clearly seen in the SEM, but also in the TEM projections. In addition, also the sorption data are in agreement with such an open system.

HR-TEM and HR-SEM micrographs of Co_3O_4-100 that had been obtained from KIT-6-100 (with higher aging temperature) are given in Figure 5a−c. In comparison with Co_3O_4-40, Co_3O_4-100 has a lower pore size and larger individual crystallite size, corresponding to the larger pores and lower wall thickness of the KIT-6-100. The average crystallite size of Co_3O_4-100 is around 8 nm. Because of the high interconnectivity between the two channel systems of the parent template, nanocast Co_3O_4-100 has a coupled framework, since the cobalt material in the two pore systems is collected in the same sample regions, irrespective of the pore system. This can be seen with unprecedented clarity in the HR-SEM images (Figure 5b,c): both pore systems of the mesoporous Co_3O_4-100 are interpenetrated, resulting in a rather dense structure, which is the clear visual correspondence of the sorption data shown in Figure 3, in which there is no pronounced capillary filling step. We have also investigated the topology of the Co_3O_4-KIT-6 composite before removal of the silica with NaOH solution. HR-SEM image of the Co_3O_4-100 before the silica removal is shown in Figure 5d. As one can see from the image, the structure is quite dense and the pores seem to be filled with Co_3O_4. Some larger bulk Co_3O_4 particles were also observed in the materials. However, after removal of the silica, we could not detect any bulk material in the ordered mesoporous Co_3O_4. Because the unstructured Co_3O_4 bulk particles have sizes around 50 nm, these particles are probably removed during the filtration process.

The extreme example of this series is Co_3O_4-135, which was produced from the template with the biggest pore size. HR-

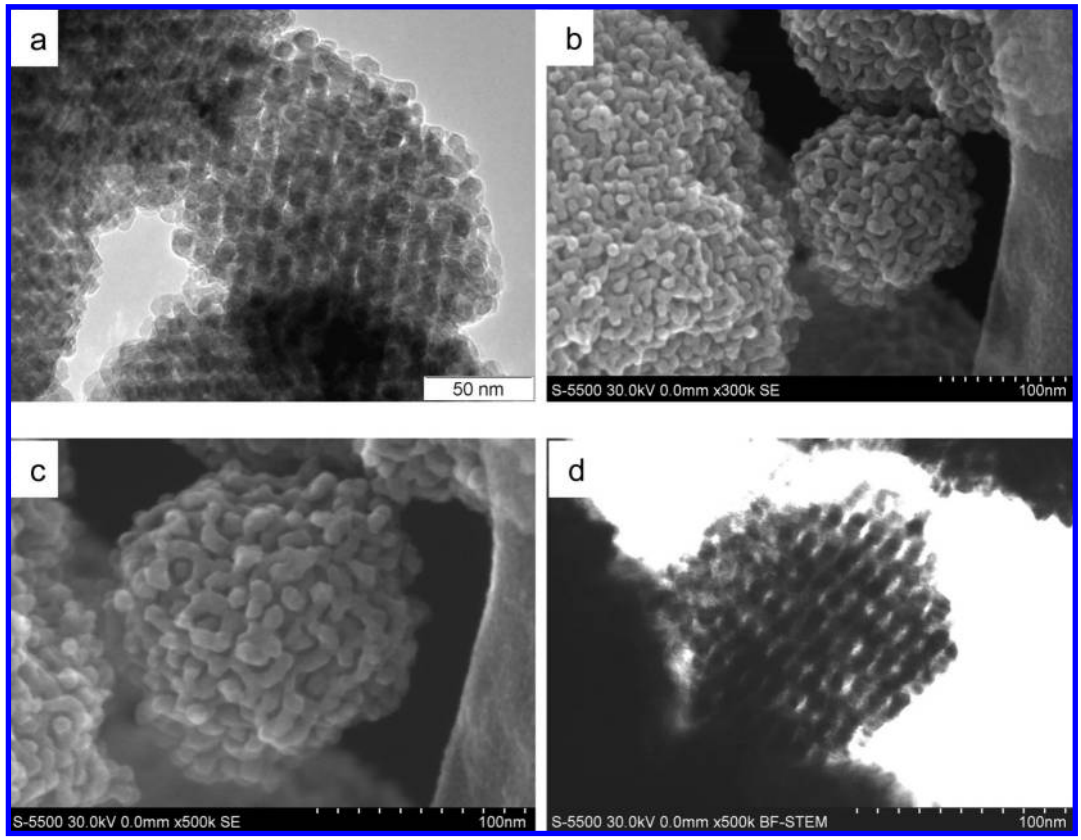

Figure 6. HR-TEM (a), HR-SEM (b,c), and STEM (d) images of Co_3O_4-135.

TEM and STEM images indicate an ordered structure (Figure 6a and d). TEM and SEM investigations were used to determine average crystallite sizes of the particles forming the network, and it was found to be around 10 nm. The topology of the Co_3O_4-135 is similar to Co_3O_4-100. Because both enantiomeric channel systems of the KIT-6 template are fully connected with each other through micropores in the silica walls, the Co_3O_4 cast consists of the completely interwoven oxide structures fully replicating the previous channel system.

We have also synthesized a cubic ordered mesoporous Co_3O_4/$CoFe_2O_4$ composite. This material could be rather interesting from a magnetic point of view due to the close coupling of an antiferromagnet and the ferromagnetic $CoFe_2O_4$. In this article, the structures and topologies of the samples are in the focus of the attention, and the results of investigations on magnetic properties of the samples are the subject of further studies. The XRD pattern shows the [211], and additionally [100] reflections, like for Co_3O_4-40, which was expected because of the low interconnectivity of the used template. Because of similar lattice parameters of Co_3O_4 and $CoFe_2O_4$, especially in case of small particles, one cannot distinguish these two phases from each other with XRD measurements (for low and wide angle XRD patterns of the composite, see Supporting Information Figure S4). However, our Moessbauer spectroscopy measurement (here not shown) revealed the presence of the $CoFe_2O_4$ phase. Representative HR-TEM and HR-SEM micrographs of Co_3O_4/$CoFe_2O_4$ composite are displayed in Figure 7. The mesoporous structure is well ordered and in accordance with the reduced symmetry of the cubic KIT-6 template; that is, the different pore systems are replicated independently. The material is highly ordered, and no unstructured bulk phase could be identified in the TEM or in SEM measurements. HR-SEM and DF-STEM images give an overview of the perfection of the structure of the ordered mesoporous composite and allow a very clear three-dimensional impression of the topology (Figure 7c and d). The average individual crystallite size of the oxide nanoparticles connected to form the mesostructure, which was obtained from measurements on different particles, is around 6.5 nm. N_2 sorption analysis reveals a broad pore size distribution (centered at 6 nm), while HR-SEM images show a pore size distribution around 10 nm (Figure 7b and d). Replication of KIT-6 aged at low temperature often results in replicas where only one of the two pores systems is replicated. Because the lack of communication between the channel systems prevents aggregation of material in the same part of the parent silica in both pore systems, only one is replicated and rather open structures result. This is different, when the two pore systems are connected at frequent intersections, thus resulting in the formation of rather dense nanocasts. Early studies indicated that when metal oxides grow only in one of the channels of KIT-6, nanocast metal oxides show a bimodal pore size distribution.[27,28] Similar effects were also described for the replication of the pore system of MCM-48 by Pt.[29,30]

Conclusions

In conclusion, we have obtained unprecedented resolution in images of the surface and near surface regions of ordered

(27) Dickinson, C.; Zhou, W.; Hodgkins, R. P.; Shi, Y.; Zhao, D.; He, H. *Chem. Mater.* **2006**, *18*, 3088.
(28) Jiao, F.; Hill, A. H.; Harrison, A.; Berko, A.; Chadwick, A. V.; Bruce, P. G. *J. Am. Chem. Soc.* **2008**, *130*, 5262.
(29) Hyun, J. S.; Ryoo, R.; Liu, Z.; Terasaki, O. *J. Am. Chem. Soc.* **2001**, *123*, 1246.
(30) Terasaki, O.; Ohsuna, T. *Top. Catal.* **2003**, *24*, 13.

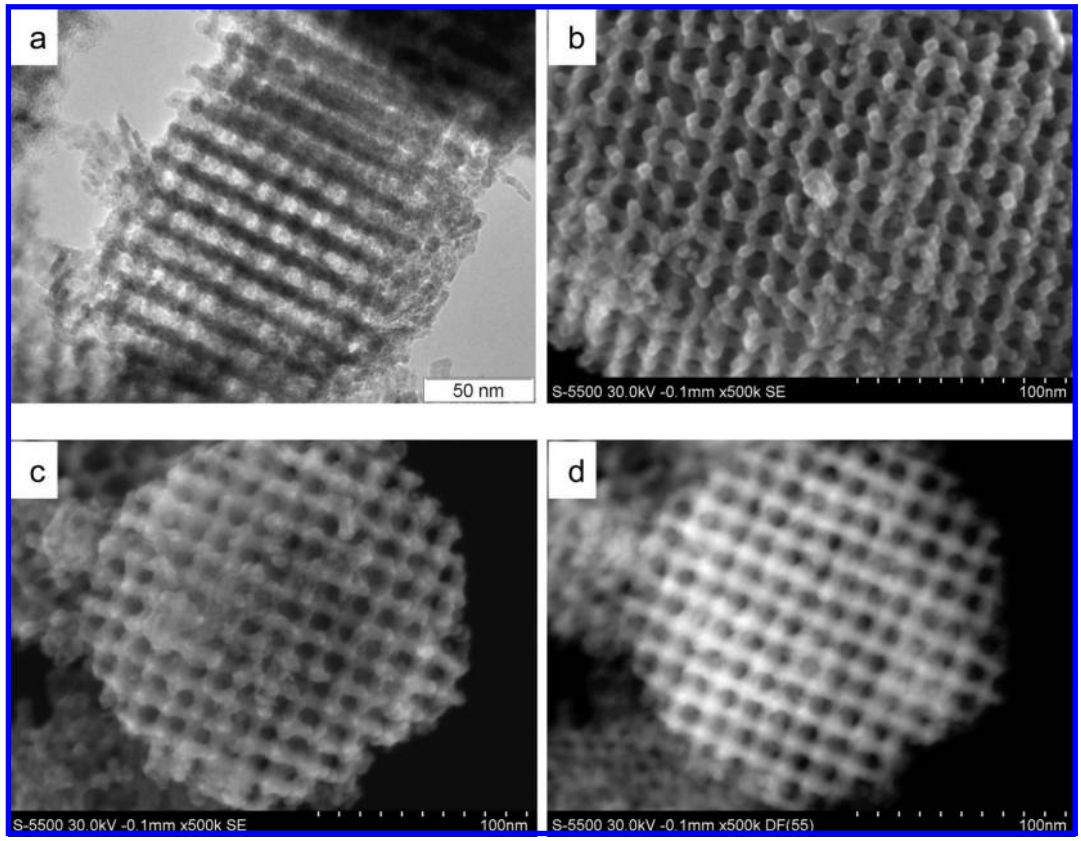

Figure 7. HR-TEM (a), HR-SEM (b,c), and DF-STEM (d) images of a mesoporous $Co_3O_4/CoFe_2O_4$ composite.

mesoporous silica by using the low voltage HR-SEM technique in combination with DF-STEM and extremely high resolution. The real space images obtained allow a much better understanding of the pore topologies of such samples and a rationalization of the results of nanocasting procedures from KIT-6 molds aged at different temperatures. The images reveal that access to the pore system from the surface should be facile, because the structure basically extends undisturbed to the surface of the material. These findings will allow a better understanding of the accessibility of the pore systems of ordered mesoporous materials and of the pore filling and replication processes, if such materials are used as molds for a nanocasting process. We could clearly show the influence of the template properties on the structure of the nanocast metal oxides. It has been demonstrated that the HR-SEM technique can give unprecedented and clear insight into the structures of such materials, and many other applications of the method seem possible. Because the method reveals Z-contrast in the dark field mode, investigation of supported metal nanoparticles on the surface of such structured supports could be especially interesting as has been shown in the studies of Bore et al.,[18] and further studies are in progress in our laboratory.

Acknowledgment. We thank B. Spliethoff for the HR-TEM images and J. Rust for the modeling of the cubic structure. We would like to thank A. H. Lu for fruitful discussions. This work was supported partially by the Leibniz Program of the DFG.

Supporting Information Available: Low angle XRD patterns, nitrogen adsorption−desorption isotherms, and pore size distribution for ordered mesoporous silica. Low angle XRD patterns of Co_3O_4, and low and wide angle XRD patterns for $Co_3O_4/CoFe_2O_4$ composite. This material is available free of charge via the Internet at http://pubs.acs.org.

JA803362S